Analytical Experiment of Time Evolution of Deceleration Effect in Traveling Wave Direct Energy Converter Using Dual-Frequency Modulation*)

Kazuhiro SHIBATA, Hiroki SATO, Hiromasa TAKENO, Kazuya ICHIMURA, Satoshi NAKAMOTO and Yousuke NAKASHIMA[1)]

Graduate School of Engineering, Kobe University, Kobe 657-8501, Japan
[1)]*Plasma Research Center, University of Tsukuba, Tsukuba 305-8577, Japan*

(Received 10 September 2018 / Accepted 10 December 2018)

Traveling wave direct energy converter (TWDEC) was proposed as an efficient energy recovery device for D-^{3}He fusion power generation. It is designed to convert the kinetic energy of 14.7 MeV protons produced by fusion reaction and is based on the inverse process of a linear accelerator. It consists of a modulator and a decelerator. In modulation process, dual-frequency modulation was proposed to improve bunching. Following to the proposal, deceleration experiment was performed, where the conditions of conventional and proposed methods were in a sequence. The result included other effects such as time variation of modulation effect, thus the effect of dual-frequency modulation to deceleration has not been clarified yet. In this work, the deceleration experiment was performed with conventional and proposed methods independently. In addition, time variation of deceleration effect was observed to exclude the time variation of the modulation effect. As a result, the effect of dual-frequency modulation to deceleration process was observed clearly. Higher efficiency was obtained with dual-frequency modulation.

Keywords: D-^{3}He fusion power generation, TWDEC, dual-frequency modulation, deceleration

DOI: 10.1585/pfr.14.2405027

1. Introduction

In D-^{3}He fusion power generation, most of produced energy is carried as kinetic energy of charged particles. Thus, high efficiency can be expected by applying direct energy converters (DECs) [1]. The DECs consist of a cusp-type dirtect energy converter (CuspDEC) [2] and a traveling wave direct energy converter (TWDEC) [3]. The CuspDEC is placed in the upstream, and designed to discriminate thermal ions and electrons from plasma flowing out from a reactor. These particles are gathered into collector, and those energy is converted into DC power. The TWDEC is placed in the downstream, and designed to convert kinetic energy of 14.7 MeV protons. Its principle is based on the inverse process of a linear accelerator. The TWDEC consists of a modulator placed in the former stage and a decelerator placed in the latter stage. The protons are incident into the modulator and bunched up in the downstream by velocity modulation. The bunched protons are introduced into the decelerator and induce traveling wave field by electrostatic induction on passing through deceleration electrodes. The protons are trapped and decelerated by the traveling wave, and the reduced kinetic energy is converted into RF power.

According to the theory of constant deceleration [4] used for design of the decelerator, high efficiency can be expected for sufficient trapping of ions provided by better bunching and narrower energy spread. In the modulation, single sinusoidal wave was used conventionally, and this scheme does not necessaarily provide complete bunching. The use of dual-frequency for modulation was proposed to improve bunching [5]. To achieve an ideal spatial bunching, in which all particles incident during one RF period gather at the same spatial position at the same time, a necessary waveform of electric field was derived analytically. This ideal waveform is similar to sawtooth waveform, and it cannot be used in practice as it needs extrenly high voltage in high frequency. An approximated scheme using combination of two components of fundamental and second harmonic frequencies was taken, and this scheme was called the dual-frequency modulation. The bunching effect of the proposed scheme was examined [5], and the research of the optimization of dual-frequency modulation has been continuing.

On one hand, deceleration experiments with dual-frequency modulation were performed. In the experiment, compared modulation schemes performed sequentially, so the results contained temporal variation of modulation effect [6] although better deceleration efficiency were shown for dual-frequency modulation. The last experiment did

author's e-mail: 179t233t@stu.kobe-u.ac.jp
*) This article is based on the presentation at the 12th International Conference on Open Magnetic Systems for Plasma Confinement (OS2018).

not distinguish pure effect only by dual-frequency modulation scheme [7]. Thus, the effect of dual-frequency modulation to deceleration process has not been clarified yet.

The purpose of this research is examination of the effects of dual-frequency modulation to deceleration process experimentally. Based on the theory of constant deceleration, we designed the decelerator for an experimental simulator with dual-frequency modulation. Then we performed experiments and analysis on deceleration effect to dual-frequency modulated particle beam with excluding time evolution of modulation effect using the simulator.

In Sec. 2, the experimental setup and evaluation methods are shown. Overview of the TWDEC simulator and experimental procedure are explained. Measurement devices and evaluation are also explained. In Sec. 3, experimental results comparing between single sinusoidal modulation and dual-frequency modulation are shown, and discussion is also presented. In Sec. 4, conclusion of the paper is given.

2. Experimental Setup

2.1 TWDEC experimental device

A schematic view of the experimental simulator is shown in Fig. 1. The device consists of sections of ion source, extraction, modulation, deceleration, and measurement. These sections are placed coaxially.

In the ion source section, a helium plasma is generated by supplying an RF power of 15 MHz to an RF antenna. The amplitude of the power is modulated by 667 Hz repetitive pulse with 67% duty ratio.

In the extraction section, extraction voltage denoted by V_{ex} is applied to an extraction electrode placed at the end of the ion source section. The helium ions are extracted and have an energy corresponding to V_{ex}. The extracted ions are bundled into a beam shape by appling V_c to a cylindrical focusing electrode placed in the downstream of the extraction electrode.

The modulator consists of four disk electrodes with a hole covered by mesh. A sinusoidal wave voltage of 7 MHz (V_{mod1}) and synchronized one of 14 MHz with leading phase difference of 0.57π rad (V_{mod2}) are applied to the second (M_2) and third (M_3) electrodes, respectively, and other electrodes are grounded. The intervals of the electrodes are the same as the quarter wavelength corresponding to 7 MHz.

The decelerator was designed based on the theory of constant deceleration [4]. According to the theory, potential well of traveling wave with constant deceleration traps bunched ions. When trapped ions increase by better bunching effect, the efficiency of TWDEC is expected to be higher. In the actual structure of the decelerator which consists of six disk electrodes with a hole covered by mesh, the traveling wave are excited by applying deceleration voltages of 7 MHz (V_{dec}) synchronized with that of modulator to 6 electrodes (D_1-D_6). By using terminal voltage of delay lines, the phase of each electrode voltage is lagging with 0.5π against that of the former one. Axial distance of electrodes installed in the decelerator from bunching position is shown in Table 1. In this structure, deceleration of appplied traveling wave is taken to be 5.5×10^{11} m/s^2.

2.2 Measurement and evaluation

At the end of the device, a Faraday cup is installed which consists of an ion repeller grid (IR), a secondary electron repeller grid (SER) and an ion collector electrode (C). The ions are discriminated for each energy by applying sweeping voltage (V_{IR}) to the IR. In the experiment, collector current I_c discriminated for each energy is obtained.

The distribution function of the ions $f(E)$ is given by $f(E) = V_{IR}^{-1/2}\,(\mathrm{d}I_c)\,/\,(\mathrm{d}V_{IR})|_{V_{IR}=E/e}$. E and e means ion energy and unit charge, respectively. The average energy of the ions are given by $\langle E\rangle = \int_0^\infty E \cdot f(E)\mathrm{d}E / \int_0^\infty f(E)\mathrm{d}E$. We used deceleration rate defined by $\eta_{dec} = (\langle E_0\rangle - \langle E\rangle)\,/\langle E_0\rangle$ for evaluation of deceleration effect. $\langle E_0\rangle$ means the average energy of incident ions.

In the experiment, a multi-point boxcar integrator (MPB) was used to obtain time variation of energy distribution. The MPB was developed by authors [6]. The timing chart of RF applications and sampling by MPB in the actual experiment is shown in Fig. 2. When we take

Table 1 Axial distance of deceleration electrodes from bunching position.

Electrodes	D_1	D_2	D_3	D_4	D_5	D_6
Position [mm]	0	9	18	26	34	41

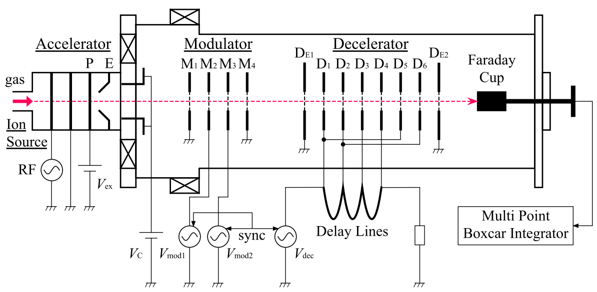

Fig. 1 Experimental simulator.

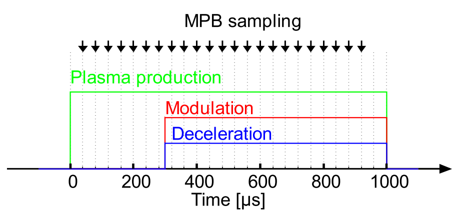

Fig. 2 Timing chart of RF applications and MPB sampling.

the origin of time at the start of the plasma production, both the modulation and the deceleration start at 300 µs and continue for 700 µs. During plasma production, the MPB sampling is performed every 40 µs until 920 µs.

3. Experimental Results & Discussion

3.1 Energy distribution function

Energy distributions of the ions in modulation process and that in deceleration process are shown in 3.1.1 and 3.1.2, respectively. For all measurements, $V_{ex} = 1.6$ kV and $V_c = 300$ V. Energy distribution functions of the ions was derived from I-V characteristics at 920 µs when the time variation of the signal stopped sufficiently.

3.1.1 Modulation process

The energy distributions of the single sinusoidally modulated particle beam and the dual-frequency modulated one are shown in Fig. 3 and Fig. 4, respectively. In these figures, the energy distribution function of the incident ion beam is denoted by dashed curve. Note that ordinate is scaled by 1/4. The ions distributed around 1.8 keV corresponding to V_{ex}. The energy distribution function of the modulated ion beam is denoted by solid curve. For the single sinusoidal modulation of Fig. 3, the ions around 1.8 keV decrease and those in the range of 1.5 - 2.1 keV appear. The components around 1.6 keV and 2.0 keV are more than that around 1.8 keV, so FWHM of the distribution is over 0.4 keV. For the dual-frequency modulation of Fig. 4, the component of 1.8 keV is more than those in other energy range, and FWHM is less than 0.2 keV.

These results are considered qualitatively as follows. Figure 5 shows a sinusoidal waveform (blue) and an approximated dual-frequency one (red). If time passing through the modulation field region is short, variation of particle energy depends on intensity of the electric field on incident timing. We roughly discuss by dividing the energy range into two: high and low ranges as shown in the figure, where the boundary is taken to be +/−0.5 as an example.

As for high energy range, the corresponding period of the dual-frequency waveform (red solid arrows) is narrower than that of the sinusoidal waveform (blue solid arrows). The number of incident particles is proportional to time period, so particles whose energy are greatly changed under the dual-frequency modulation are fewer than those under the sinusoidal modulation. As for low energy range, wider period of the dual-frequency waveform (red dotted arrows) than that of the sinusoidal waveform (blue dotted arrows) results in more particles with small change in energy.

This consideration agrees with the difference of energy distribution shown in Figs. 3 and 4. The period of high energy range in the dual-frequency modulation is affected by the short period of second harmonic frequency, while the long period of the fundamental frequency determines that in the single sinusoidal modulation.

From those results, it can be said that averaged energy spread of ions decreases when dual-frequency modulation is applied.

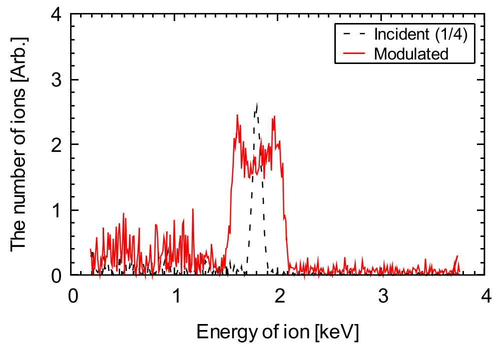

Fig. 3 Energy distribution of modulated ions by single sinusoidal wave. Conditions of RF voltages are V_{m1} = 190 V_{0p}, V_{m2} = 0 V_{0p}, V_{dec} = 0 V_{0p}. (V_{0p}: zero-to-peak voltage)

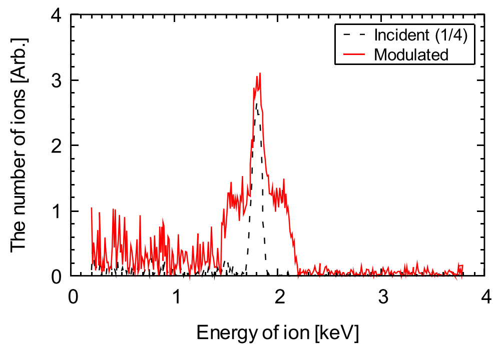

Fig. 4 Energy distribution of modulated ions by dual-frequency wave. Conditions of RF voltages are V_{m1} = 190 V_{0p}, V_{m2} = 100 V_{0p}, V_{dec} = 0 V_{0p}.

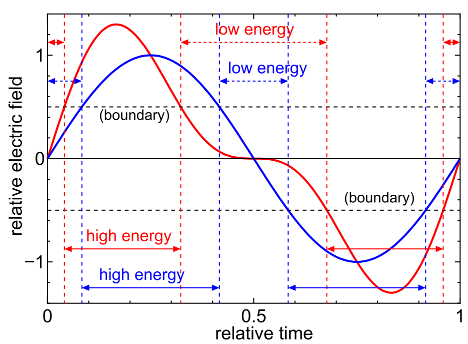

Fig. 5 Energy ranges and corresponding periods for sinusoidal waveform (blue) and approximated dual-frequency one (red).

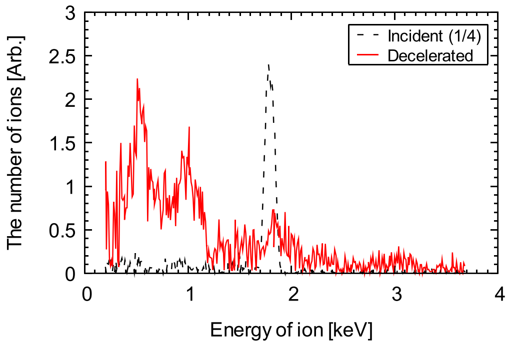

Fig. 6 Energy distribution of decelerated ions with single sinusoidal modulation. Conditions of RF voltages are V_{m1} = 190 V_{0p}, V_{m2} = 0 V_{0p}, V_{dec} = 220 V_{0p}.

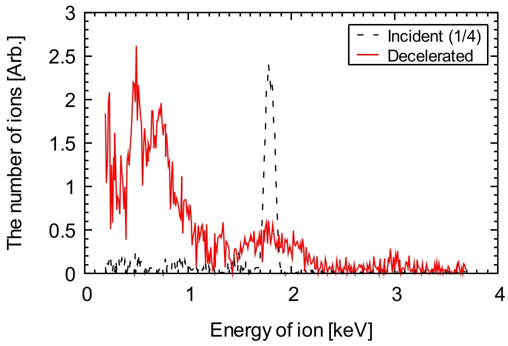

Fig. 7 Energy distribution of decelerated ions with dual-frequency modulation. Conditions of RF voltages are V_{m1} = 190 V_{0p}, V_{m2} = 100 V_{0p}, V_{dec} = 220 V_{0p}.

3.1.2 Deceleration process

The energy distribution functions of decelerated ion beam with single sinusoidal modulation and dual-frequency modulation are shown in Fig. 6 and Fig. 7, respectively. Dashed curves are the same as those in Figs. 3 and 4, and solid ones mean ions with modulation and deceleration.

According to Fig. 6, the particles around 1.8 keV significantly decrease, while those in the range of 0.2 - 1.2 keV appear when single sinusoidal modulation is applied. For dual-frequency modulation of Fig. 7, however, the low energy components, especially those in the range of 0.2 - 0.8 keV are more than those in Fig. 6. This means larger deceleration effect appears on dual-frequency modulation.

The better bunching is expected in the dual-frequency modulation, and energy spread is narrower as shown in Figs. 3 and 4, thus, dual-frequency modulated ions are well concentrated in phase space of the theory of the constant deceleration. In this situation, better deceleration effect can be expected. The results shown in Figs. 6 and 7 are consistent with this consideration.

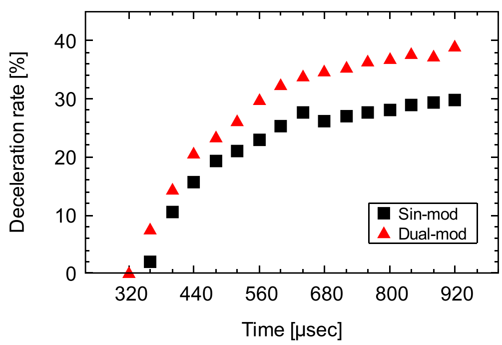

Fig. 8 Time variation of deceleration rate.

3.2 Time variation of deceleration effect

We evaluated time evolution of deceleration effect by using deceleration rate. Time variation of the deceleration rate is shown in Fig. 8. The deceleration rate increases as time epalses for both single sinusoidal modulation and dual-frequency modulation. This variation is considered to be due to time variation of modulation effect.

As for the comparison of absolute deceleration rates between single sinusoidal modulation and dual-frequency modulation, the latter one is superior to the former one for all the time of 360 - 920 μs. For the single sinusoidally modulated beam, the deceleration rate increases up to 30%. On one hand, the deceleration rate with dual-frequency modulation increases up to 39%. From this result, we clarified that the deceleration effect with dual-frequency modulation is better than that with single sinusoidal modulation.

4. Conclusion

We carried out deceleration experiments and analysis on time evolution of deceleration effect with dual-frequency modulation compared with single sinusoidal modulation. Energy distribution of the ions and the deceleration rate were used for these evaluations. As a result, we found that averaged energy spread of modulated particles with dual-frequency modulation was narrower than that with single sinusoidal modulation, which was favorable for better deceleration by constant deceleration scheme. As for deceleration effect, the consistent results with modulation effect was obtained that deceleration of dual-frequency modulated beam was also better than that of sinusoidally modulated beam. The effectiveness of dual-frequency modulation to deceleration effect was confirmed.

Acknowledgments

This work was supported in part by the bilateral coordinated research between PRC, Univ. Tsukuba, NIFS, and Kobe Univ. (NIFS13KUGM082), and was also supported in part by a Grant-in-Aid for Scientific Research (B) (16H04317) from JSPS.

[1] Y. Tomita *et al.*, Nucl. Instrum. Methods Phys. Res. A **402**, 421 (1998).
[2] H. Momota *et al.*, Proc. 7th Int. Conf. Emerging Nucl. Energy Systems, 16 (1993).
[3] H. Momota, LA-11808-C, Los Alamos Natl. Lab., 8 (1990).
[4] Y. Togo *et al.*, Plasma Fusion Res. **10**, 3405013 (2015).
[5] H. Sato *et al.*, Joint meeting of 26th International Toki Conference and 11th Asia Plasma and Fusion Association Conference, P1-99 (2017).
[6] H. Takeno *et al.*, 10th Joint Convention of Fusion Energy, p.20-130 (2014).
[7] K. Shibata *et al.*, Plasma Conference 2017, 24P-90 (2017).